Optimization of a Six-Zone Simulated-Moving-Bed Chromatographic Process

Young-Il Lim*

Department of Chemical Engineering, Hankyong National University, Anseong, 456-749 Korea

Sten Bay Jørgensen

CAPEC, Department of Chemical Engineering, Technical University of Denmark, 2800 Kgs. Lyngby, Denmark

Using strong cation-exchange simulated-moving-bed (SMB) chromatography, a nitrogen−phosphate−potassium (NPK) fertilizer is produced in a cost-effective manner. The SMB process, operated in a nontraditional way, is divided into production and regeneration sections, for exclusion of undesirable ions, and is composed of six zones, including two wash-water zones. This paper addresses modeling, simulation, and optimization studies on this ion-exchange SMB process, based on experimental data obtained both from a pilot plant and an industrial plant. Model parameters that are initialized by empirical equations are identified, comparing the simulation results with the experimental data. Through sensitivity analysis of the model parameters, their effects on the process performance are examined. The simulation results show good agreement with in situ experimental data obtained in both the pilot- and industrial-scale plants. The objectives of this study are to optimize the SMB process in terms of (i) maximization of productivity in the production section and (ii) minimization of wash-water consumption, thereby resulting in (i) an increase in profit and (ii) a reduction in the overall operating cost in the downstream processing, respectively. The two objectives are sequentially treated within the framework of a multilevel optimization procedure (MLOP), which includes two pre-optimization levels, a productivity maximization level, and a desorbent (or wash-water) consumption minimization level. In this optimization study, it is demonstrated that wash-water consumption can be reduced by 5% at a 5% higher productivity.

1. Introduction

Simulated-moving-bed (SMB) chromatography is a powerful technique used to continuously separate multiple components in large amounts, and it is useful for a preparative scale. Thus, the SMB process constitutes an interesting alternative to conventional batch chromatography and has recently gained an increased impact.[1] The SMB chromatography usually works with the inherent advantage of a high driving force, resulting in low solvent consumption, small apparatus scale, and high yields. However, to take full advantage of this principle, a large number of operational parameters (e.g., flow rate, switching time, and column configuration) must be properly adjusted.[2]

For mathematical modeling and computer simulation of SMB systems, several different models are used, including the true-moving-bed (TMB) model,[3,4] the continuous-moving-bed (CMB) model for linear systems,[5,6] and the SMB model.[1,7,8] However, the quality of the solution of the TMB or CMB model is only sufficient for a restricted range of applications.[1] The SMB model with periodic port movement in the flow direction is more realistic than the TMB or CMB models[5] but requires a longer calculation time.[9] However, the SMB model with periodic port movement may not be suitable for repeated runs in optimization procedures.[4]

A packed-bed chromatographic separation can be described by convection-dominated parabolic partial differential equations (PDEs) for mass conservation in the mobile phase, ordinary differential equations (ODEs) for the solute adsorption in the stationary phase, and, eventually, algebraic equations (AEs) for the adsorption isotherm between the two phases. Thus, the combined models lead to a nonlinear and coupled partial differential algebraic equation (PDAE) system which is often solved, after discretization of spatial derivatives, by ODE or DAE (differential algebraic equation) time integrators (e.g., DASSL[10]) in the framework of the method of lines (MOL).[4,5,8,11−13] The MOL procedure converts the distributed dynamic system to a large system of ODEs or DAEs, which often requires a long computational time and may result in substantial discretization error.[14]

A conservation element and solution element method[14−17] (the CE/SE method, for short) has been proposed to solve the distributed dynamic system (or PDEs) accurately and effectively. The CE/SE method enforces both local and global flux conservation in space and time, using Gauss's divergence theorem, and uses a simple stencil structure (two points at the previous time level and one point at the present time level) that leads to an explicit time-marching scheme.[17]

A nitrogen−phosphate−potassium (NPK) fertilizer process has been designed and operated by Kemira Denmark A/S in a cost-effective manner, using SMB chromatography packed with a strong cation-exchange resin ($D_c \times L_c = 2$ m $\times$ 1.8 m, 16 columns). This SMB process exhibits several characteristic features:

(1) The feed solution is a strong electrolyte, i.e., an acid solution of ∼10 equiv/L (1 equiv/L = 1 equivalent mol/L) with nonlinear adsorption isotherms;

(2) A nonequilibrium adsorption model should be considered, because of a strong mass-transfer effect within large resin particles;

(3) It contains six zones including two wash-water zones for ion exclusion, which divide the process into production and regeneration sections (see Figure 1);

(4) The process with 16 columns is pre-operated for 5 h with a switching time of 5 min to reach a cyclic stationary state;

* To whom correspondence should be addressed. Tel.: +82 31 670 5207. Fax: +82 31 670 5445. E-mail: limyi@hknu.ac.kr.

10.1021/ie0613772 CCC: $37.00
Published on Web 04/28/2007

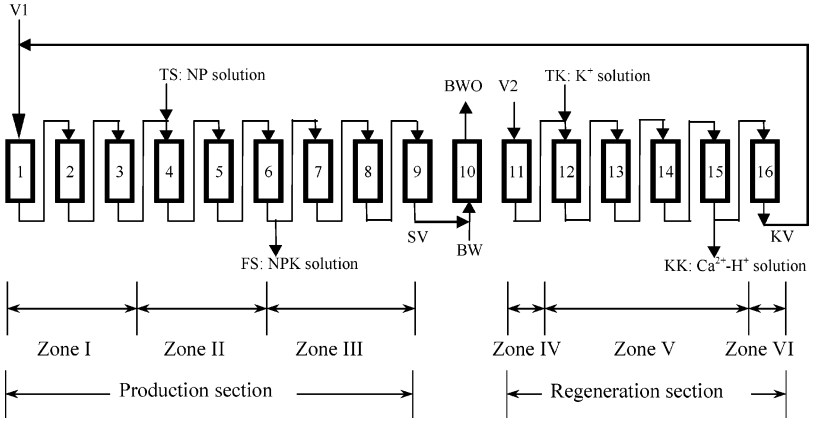

Figure 1. Schematic of the 16-column configuration (3/3/3−1-1/4/1) for a nitrogen−phosphorus−potassium (NPK) ion-exchange simulated-moving-bed (SMB) process.

(5) Steep or discontinuous concentration profiles appear in several places; and

(6) A modest purity requirement of the resulting product solution is sufficient to minimize the losses of valuable components.

Features (1)−(3) and (6) render this SMB process nonstandard; thus, a model is developed to investigate different aspects of this SMB operation and to optimize the process. A nonlinear and nonequilibrium SMB model[1,7,8] is developed in this study and the CE/SE method[14,17] is used to ensure fast and accurate calculation.

This article reports both experimental and simulation studies on the nontraditional ion-exchange SMB process for chloride-free NPK fertilizer production.[18] The study intends to optimize the SMB process to reduce wash-water consumption and increase productivity within a given purity, which will result in reducing the operating cost of downstream evaporation and drying processes.

The remainder of the paper is organized as follows. Section 2 describes the specific SMB process. Section 3 presents mathematical models and model parameters. Simulation and optimization results are analyzed in section 4, through comparison with experimental data. The conclusions are presented in section 5.

2. Process Description

While conventional NPK fertilizers usually contain large amounts of chloride, as a result of the introduction of the necessary potassium content as KCl, the $Ca^{2+}-H^{+}-K^{+}$ ion-exchange SMB process operated at Kemira A/S in Denmark had been designed to produce chloride-free fertilizer.[18] The raw materials normally used in the manufacturing of NPK fertilizers are nitric acid for nitrogen (N), calcium phosphate for phosphate (P), and potassium chloride for potassium (K). The two unwanted elements are calcium and chloride. Calcium is removed via cation exchange between Ca^{2+} and K^{+} and the chloride, as an anion, is excluded from the product by separating the production section from the regeneration section.

A cation-exchange reaction between counter-ions Ca^{2+}, H^{+}, and K^{+} occurs on a strong cation-exchange resin (macroporous Purolite 160C, with a particle size of $d_p = 0.675 \times 10^{-3}$ m and an average pore diameter of 1.0×10^{-7} m):

$$Ca^{2+}_{(aq)} + 3KR_{(resin)} + H^{+}_{(aq)} \leftrightarrow CaR_{2(resin)} + HR_{(resin)} + 3K^{+}_{(aq)} \quad (1)$$

In Figure 1, a 16-column arrangement is shown. There are two feed solutions (TS and TK), two wash water solutions (V1 and V2), product and regenerated solutions (FS and KK), and two slip water solutions (SV and KV). KV is totally recycled to V1. It is important that operating conditions are adjusted such that the KV stream does not contain ions (e.g., Ca^{2+} and Cl^{-}). SV is only used for backwashing (BW). The BW column serves to remove nitrate ions and to clean the resin particles, which could be contaminated by the feed solution impurities. After one cycle period, all positions are shifted in the direction of the liquid flow. For this SMB system, several rounds (1 round = 16 shiftings) are required to reach a periodic stationary state.[7]

In the production section (V1−TS−FS−SV), which includes zones I, II, and III, calcium and hydrogen ions ($Ca^{2+}-H^{+}$) are removed from the feed solution, which contains dissolved phosphate rock with nitric acid (TS), through adsorption of Ca^{2+} and H^{+} on the resin. At the same time, potassium ions (K^{+}) are desorbed from the resin. Hence, the product solution (FS) contains the three desired NPK components (NO_3^{-}, PO_4^{3-}, K^{+}). In the regeneration section (V2−TK−KK−KV), which includes zones IV, V, and VI, the adsorbed calcium and hydrogen ions ($Ca^{2+}-H^{+}$) are replaced by K^{+} ions by feeding the KCl solution (TK). For simplicity, the ternary system is considered as a binary system, assuming that the first component is $Ca^{2+}-H^{+}$ and the second component is K^{+}. This simplifying assumption is reasonable in practice, because the main objective of the process is to add K^{+} into the feed solution (TS), while removing both Ca^{2+} and H^{+}. The purity of the K^{+} ion in the FS solution is one of the most important indicators for the process performance.

The BW column is not modeled in this simulation study. In the model development described below, 15 columns are considered. These are grouped into 6 zones, such as wash water zone I (3 columns), production zone II (3 columns), slip water zone III (3 columns), another wash water zone IV (1 column), regeneration zone V (4 columns), and another slip water zone VI (1 column), as shown in Figure 1. The column configuration is described by the number of columns for each zone, expressed as [3/3/3−1−1/4/1], which is a typical column configuration for the industrial-scale plant; however, various modified column configurations are possible. The six-zone SMB process is different from a traditional four-zone SMB process, in the sense that there exist two wash-water zones (zones I and IV in Figure 1) to enable Cl^{-}- and NO_3^{-}-free operation in the production and regeneration sections, respectively. Therefore, the SMB process can be considered as ion-exclusion and ion-exchange chromatography.

Table 1. Operating Conditions and Simulation Parameters for the Pilot SMB Plant[a]

	Production Section			Regeneration Section		
parameter	zone I	zone II	zone III	zone IV	zone V	zone VI
Q (L/min)	2.14	2.56	1.44	2.26	3.02	1.26
v_L (m/min)	0.494	0.591	0.332	0.521	0.697	0.291
D_{ax} (m^2/min)	$0.02v_L$	$0.02v_L$	$0.02v_L$	$0.02v_L$	$0.02v_L$	$0.02v_L$
k (min^{-1})	0.40	0.40	0.40	0.70	0.70	0.70
Peclet number, Pe[b]	105	105	105	105	105	105
Stanton number, St[c]	1.71	1.43	2.54	2.83	2.12	5.07

parameter	value
column information	
length, $L_{c,eff}$	2.107 m[d]
D_c	0.1 m
bed voidage, $\epsilon_{b,eff}$	0.5522[e]
number of columns	15 (2/5/2−1/4/1)[f]
inlet concentration, C_{in}	
at V1	$C_{in,A} = C_{in,B} = 0$ equiv/L
at TS	$C_{in,A} = 9.93$ equiv/L, $C_{in,B} = 0.01$ equiv/L
at V2	$C_{in,A} = C_{in,B} = 0$ equiv/L
at TK	$C_{in,A} = 0.11$ equiv/L, $C_{in,B} = 3.82$ equiv/L
simulation parameters	
mesh number, N_m	26
shifting time, τ	5 min
shifting number, N_{shift}	53
resin capacity, $n_{T,p}$[g]	3.17

[a] V1/TS/FS − V2/TK/KK = 10.7/2.1/5.6−11.3/3.8/8.8 L/cycle. [b] $Pe = L_{c,eff}v_L/D_{ax}$. [c] $St = L_{c,eff}k/v_L$. [d] $L_c = 1.492$ m. [e] $\epsilon_b = 0.37$ and $V_{dead} = 4.77$ L. [f] One backwashing column is not taken into account. [g] The term $n_{T,p}$ ($n_{T,p} = n_T/(1 - \epsilon_b)$) has units of equiv/L, based on the particle volume, whereas the parameter n_T ($n_T = 2.0 \pm 0.1$) is based on the bed volume.

Table 2. Operating Conditions and Simulation Parameters for the Industrial-Scale SMB Plant[a]

	Production Section			Regeneration Section		
parameter	zone I	zone II	zone III	zone IV	zone V	zone VI
Q (m^3/min)	0.94	1.174	0.768	1.066	1.506	0.552
v_L (m/min)	0.541	0.676	0.442	0.614	0.868	0.318
D_{ax} (m^2/min)	$0.04v_L$	$0.04v_L$	$0.04v_L$	$0.04v_L$	$0.04v_L$	$0.04v_L$
k (min^{-1})	0.40	0.40	0.40	0.70	0.70	0.70
Peclet number, Pe[b]	65	65	65	65	65	65
Stanton number, St[c]	1.93	1.54	2.36	2.97	2.10	5.73

parameter	value
column information	
length, $L_{c,eff}$ (m)[d]	2.605 m
D_c (m)	2.0 m
bed voidage, $\epsilon_{b,eff}$[e]	0.5527
number of columns[f]	15 (3/3/3−1/4/1)
inlet concentration, C_{in}	
at V1	$C_{in,A} = C_{in,B} = 0$ equiv/L
at TS	$C_{in,A} = 10.37$ equiv/L, $C_{in,B} = 0$ equiv/L
at V2	$C_{in,A} = C_{in,B} = 0$ equiv/L
at TK	$C_{in,A} = 0$ equiv/L, $C_{in,B} = 3.884$ equiv/L
simulation parameters	26
mesh number, N_m	5
shifting time, τ (min)	53 min
shifting number, N_{shift}	
resin capacity, $n_{T,p}$[g]	3.17

[a] V1/TS/FS−V2/TK/KK = 4.7/1.17/2.03−5.33/2.20/4.77 m^3/cycle. [b] $Pe = L_{c,eff}v_L/D_{ax}$. [c] $St = L_{c,eff}k/v_L$. [d] $L_c = 1.85$ m. [e] $\epsilon_b = 0.37$ and $V_{dead} = 2.37$ m^3. [f] One backwashing column is not taken into account. [g] The term $n_{T,p}$ ($n_{T,p} = n_T/(1 - \epsilon_b)$) has units of equiv/L, based on the particle volume, whereas the parameter n_T ($n_T = 2.0 \pm 0.1$) is based on the bed volume.

Typical design parameters, operating conditions and simulation parameters are reported in Tables 1 and 2 for two ion-exchange SMB plants; one at pilot scale and another at industrial scale, respectively. The pilot plant is designed for identifying the optimal operating conditions to be implemented in the real plant. The same feed solution and the same resin type are used in the two plants, which normally are operated at the same shifting time ($\tau = 5$ min). The production capacity of the real plant is ~500 times greater than that of the pilot plant. Despite the quite different column diameters of the two plants, the operation is conducted at a similar interstitial velocity.

Equation 1 shows the exothermic adsorption reaction. For adsorption columns (e.g., zone II in Figure 1), the temperature varies over a range of 45 °C ≤ T ≤ 55 °C, but the average temperature is assumed to be $T = 50$ °C. The resin capacity, based on the bed volume ($n_T = 2.0 \pm 0.1$ equiv/L) is experimentally confirmed. Because the resin concentration (n) is often expressed based on the resin particle volume, including

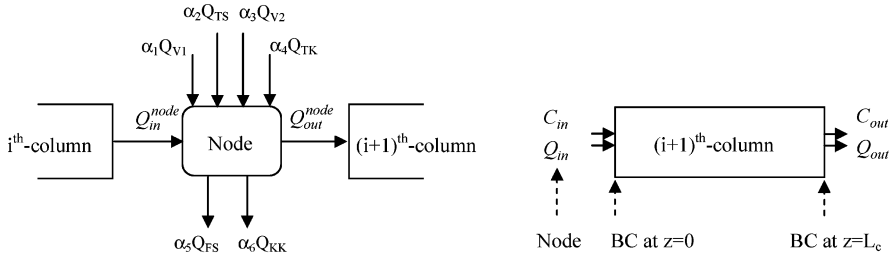

(a) Flowrates at the node (b) Node and column boundary conditions (BC)

Figure 2. Schematic of the node and column configurations in this six-zone SMB process model: (a) flow rates at the node and (b) node and column boundary conditions (BC).

the pore volume (see eq 2 in section 3), the resin capacity, based on the resin volume ($n_{T,p}$), is shown in Tables 1 and 2. In the following section, an SMB model and the model parameters in Table 1 and 2 are detailed.

3. Model Development

When mass-transfer resistance in the particle is significant for the adsorption mechanism because of the large resin particle diameter, a nonequilibrium model can be used for chromatographic column models. A packed-bed chromatographic adsorption between the stationary and mobile phases for each cation (i.e., Ca^{2+}, H^+, and K^+) leads to a PDAE system that involves one PDE equation, one ODE equation, and one AE equation. The chromatographic column model is described by

$$\frac{\partial C}{\partial t} + \frac{\partial (v_L C)}{\partial z} = \frac{\partial}{\partial z}\left(D_{ax}\frac{\partial C}{\partial z}\right) - \frac{1-\epsilon_b}{\epsilon_b}k(n^* - n) \quad (2a)$$

$$\frac{dn}{dt} = k(n^* - n) \quad (2b)$$

$$0 = n^* - g(C) \quad (2c)$$

where v_L is the interstitial velocity, D_{ax} the axial dispersion coefficient, and ϵ_b the bed voidage. The liquid and solid concentrations for each component are C and n, respectively, and n^* is the equilibrium concentration, which is normally defined as a function of the liquid concentration ($g(C)$). A conventional linear driving force (LDF) model with a lumped mass-transport coefficient (k) is used in eq 2b for the adsorption kinetics. The Peclet number ($Pe = v_L L_c/D_{ax}$) and the Stanton number ($St = kL_c/v_L$) are the important dimensionless groups that determine in the numerical characteristic steepness of the concentration profiles and stiffness of the equation system, respectively. For example, when Pe is large and St is small, the system will exhibit steep gradients in the spatial direction (z) and is nonstiff in regard to time (t). In eqs 2, two initial conditions (IC, $t = 0$) for two time derivatives and two boundary conditions (BC, $z = 0$ or L_c) for the convection and diffusion terms are required.

$$\mathrm{IC} = \begin{cases} C(z,0) = C_{\mathrm{initial}}(t = 0, \forall\, z) \\ n(z,0) = n_{\mathrm{initial}}(t = 0, \forall\, z) \end{cases} \quad (3)$$

$$\mathrm{BC} = \begin{cases} v_L(C_{z=0} - C_{in}) = D_{ax}\left.\dfrac{\partial C}{\partial z}\right|_{z=0}, \forall\, t \\ \left.\dfrac{\partial C}{\partial z}\right|_{z=L_c} = 0, \forall\, t \end{cases} \quad (4)$$

where C_{in} is the inlet concentration entering the column, which is given by the operating conditions.

The SMB process is modeled by connecting the column model (eqs 2−4) with the node model, which represents the periodic operation through the port switching.[7] Inlet concentrations (C_{in}) and the flow rate (Q_{in}) for each column are calculated from the outlet concentration (C_{out}^{node}) and flow rate (Q_{out}^{node}) in the node where perfect mixing is assumed (see Figure 2):

$$Q_{in} \equiv Q_{out}^{node} = Q_{in}^{node} + \alpha_1 Q_{V1} + \alpha_2 Q_{TS} + \alpha_3 Q_{V2} + \alpha_4 Q_{TK} - \alpha_5 Q_{FS} - \alpha_6 Q_{KK} \quad (5a)$$

$$C_{in}Q_{in} = C_{in}^{node}Q_{in}^{node} + \alpha_1 C_{V1}Q_{V1} + \alpha_2 C_{TS}Q_{TS} + \alpha_3 C_{V2}Q_{V2} + \alpha_4 C_{TK}Q_{TK} - \alpha_5 C_{in}^{node}Q_{FS} - \alpha_6 C_{in}^{node}Q_{KK} \quad (5b)$$

where α_1−α_6 are the logical variables (0 or 1), according to the port switching. Figure 2a depicts a node that connects two columns. The flow rate (Q_{out}^{node}) calculated from the node model determines the flow rate (Q_{in}) of the next column. The outlet concentration from the node model is the inlet concentration (C_{in}) to the next column. Thus, this node model, together with the switching policy, describes the SMB operations model. The two boundary conditions (eq 4) are applied at the inlet and outlet of each column, as shown in Figure 2b.

The SMB model contains several model parameters, such as bed voidage (ϵ_b), axial dispersion coefficient (D_{ax}), mass-transfer coefficient (k), and adsorption isotherms (n^*), which may be determined through experiments or empirical models.

The bed voidage (ϵ_b) is mainly related to particle packing characteristics in the column. However, in SMB plants, considerable extra-column volume (or dead volume), including distributors, collectors, connecting pipes, and valves, can be involved.[4,20] In 2000, Beste et al.[4] introduced an effective column length and effective bed voidage:

$$L_{c,eff} = \frac{V_{total}}{S} = L_c + \frac{V_{dead}}{S} \quad (6)$$

$$\epsilon_{b,eff} = \frac{V_{liquid}}{V_{total}} = \frac{\epsilon_b L_c S + V_{dead}}{L_c S + V_{dead}} \quad (7)$$

The bed voidage ($\epsilon_b = 0.37$) is assumed to be constant, ignoring resin shrinking and swelling effects during desorption and adsorption. The two effective values are substituted for L_c and ϵ_b in eqs 2−4. The effective bed voidage ($\epsilon_{b,eff}$) is larger than the bed voidage ϵ_b and the resin particles are distributed less densely in the simulation but to the same extent as that in reality.

The axial dispersion coefficient (D_{ax}) generally does not have a substantial effect on the solution of the model. However, axial dispersion will be larger than an expected value obtained from an empirical model for the single column, considering that backmixing is substantial in the connecting zones between columns.[19] In this study, the axial dispersion

coefficient is estimated to be[19]

$$D_{ax} = 0.02 v_L \qquad \text{(for the pilot plant)} \tag{8}$$

$$D_{ax} = 0.04 v_L \qquad \text{(for the real plant)} \tag{9}$$

Based on these values, the respective axial Peclet numbers ($Pe = L_{c,eff} \cdot v_L / D_{ax}$) are ~105 and ~65 for the two plants.

It is considered that the $Ca^{2+}-H^{+}-K^{+}$ ion-exchange adsorption mechanism is controlled by the intraparticle diffusion resistance, rather than the liquid film resistance, because the diameter of the resin particles that have been used is large. The LDF model is applied in this study for the intraparticle diffusion (eq 2b). The mass-transfer coefficient is set to $k_{prod} = 0.4\ min^{-1}$ for the production section and $k_{regen} = 0.7\ min^{-1}$ for the regeneration section.[19] The Stanton number ($St = kL_{c,eff}/v_L$) varies over a range of $1.4 \le St \le 5.8$ for the two plants. The sensitivity of the process performance to the model parameters will be analyzed in section 4.

3.1. Generalized Adsorption Rate Model. As mentioned previously, two wash water zones (zones I and IV in Figure 1) are arranged in the present SMB plants to achieve Cl^{-}- and NO_3^{-}-free operation. The wash-water zones can become a nonadsorption region (or reach a quasi-equilibrium state between the liquid and solid phases), when the resin contacts with the aqueous solution that contains a negligible concentration of cations (e.g., pH 6−7). Thus, both nonequilibrium regions (adsorption regions) and equilibrium regions (nonadsorption regions) are present in the NPK SMB unit.

The LDF model represents intrinsically nonequilibrium adsorption, because the actual resin concentration (n_i) cannot reach the equilibrium concentration (n_i^*), because of the mass-transfer rate (k). When adsorption kinetics has a very large k value, the LDF model is close to an equilibrium model. However, the difference between the two concentrations ($n_i^* - n_i$) is large for a small value of k, such as that in this NPK fertilizer process. Therefore, a dual adsorption kinetics model may be needed, as follows:

$$r_i \equiv \frac{dn_i}{dt} = k(n_i^* - n_i) \qquad \text{(for adsorption regions)} \tag{10a}$$

$$r_i \equiv \frac{dn_i}{dt} = 0 \qquad \text{(for nonadsorption regions)} \tag{10b}$$

The switch between the aforementioned two adsorption rate models presents a state change (or event) whenever a state condition is satisfied. The state condition of the present ion-exchange SMB system is determined by the presence of cations in the fluid. If no cations are present in the fluid, adsorption or desorption does not occur, as shown in eq 10b. This problem shows a behavior that is analogous to that of a heat conduction problem,[21] where a material undergoes a phase change at different spatial positions in time.

The discrete events in the PDAE system for the SMB process move temporally and spatially. Consequently, it is a challenge to detect when and where the adsorption region changes to the nonadsorption region, and then to interchange the adsorption kinetics. The question is how to simulate such discrete events. This problem is addressed in the presentation of the following numerical solution methodology.

To replace the LDF model (eq 2b) with eq 10 in the PDAE system, switching functions are used to detect the discrete event (or state change). A generalized rate equation based on the switching functions is proposed for the binary system, as follows:

$$\begin{cases} r_A^{general} = \phi_{sum}\phi_{product} r_A \\ r_B^{general} = -\, r_A^{general} \end{cases} \tag{11a}$$

where $r_A \equiv dn_A/dt = k(n_A^* - n_A)$, from eq 2b. The sum kernel (ϕ_{sum}) and product kernel ($\phi_{product}$) are defined for a binary system with components A and B:

$$\begin{cases} \phi_{sum} = 0 & (\text{if } C_A + C_B \le 0.0) \\ \phi_{sum} = 1 & (\text{elsewhere}) \end{cases} \tag{11b}$$

$$\begin{cases} \phi_{product} = 0 & (\text{if } C_A C_B < 0.0) \\ \phi_{product} = 1 & (\text{elsewhere}) \end{cases} \tag{11c}$$

This formulation satisfies the electroneutrality condition in the solid phase (i.e., $\sum_i r_i = 0$), as will be shown in Figure 7, and is identical to the conventional LDF model (eq 2b) in the nonequilibrium zone. It is essential that the switching functions given in eqs 11b and 11c are applicable to an explicit time integrator, such as the conservation element and solution element (CE/SE) method[14,17] that is used in this study. An alternative form of the switching function[22] is used for an implicit ODE time integrator, such as DASSL.[10]

The problem type encountered in this ion-exchange SMB unit belongs to the class of discrete events or a hybrid problem.[28] This problem type is presented by switching between the two kinetic expressions in eq 10 and implemented using the so-called generalized rate equation in eq 11 for the time-marching CE/SE scheme. This generalized model is considered as a numerical implementation rather than a physical model, which renders the generalized version of the nonequilibrium model (i.e., LDF model) feasible, even in equilibrium regions.

3.2. Adsorption Isotherms. The equilibrium concentration (or adsorption isotherm) has an important role in the column model (eq 2). The adsorption isotherm intrinsically decides separation performance. Recall that the feed solution of the NPK ion exchanger is a concentrated electrolyte solution with cations (Ca^{2+}, H^{+}, and K^{+}) and counterpart anions (NO_3^{-}, PO_4^{3-}, and eventually Cl^{-}). Because of the strong electrolyte, a nonlinear adsorption isotherm is expected.

An empirical correlation is proposed for the binary adsorption ($Ca^{2+}-H^{+}$ and K^{+}) on Purolite 160C resin as a fifth-order polynomial function fitted to the experimental data of a 3.3 N solution:

$$n_A^* = n_T x_A (2.2321 - 7.66474 x_A + 17.714 x_A^{\,2} - 18.882 x_A^{\,3} + 7.6032 x_A^{\,4}) \tag{12a}$$

$$n_B^* = n_T - n_A^* \tag{12b}$$

where the subscripts A and B denote the binary components $Ca^{2+}-H^{+}$ and K^{+}, respectively; n_T is the resin capacity; and x_A is the liquid mole fraction of A ($x_A = C_A/(C_A + C_B)$). Equation 12b implies the electroneutrality condition in the solid phase at equilibrium (i.e., $\sum_i n_i^* = n_T$). Equation 12 is used over the entire concentration range in this study. All concentrations are based on the equivalent mole concentration (equiv/L). Figure 3 illustrates the experimental points and their fitting curve at $C_{A+B} = 3.3$ N.

A more-complex model for NPK concentrated solutions can be developed based on thermodynamic equilibrium constants, for which nonideality in liquid and resin phases is taken into account.[23] Activity coefficients in the solution are calculated

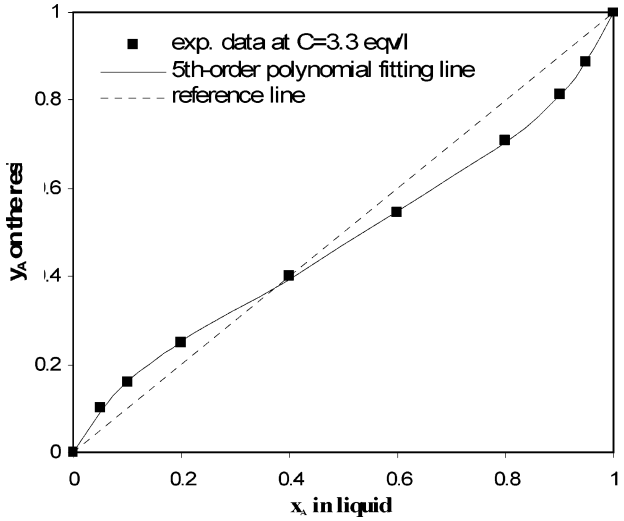

Figure 3. Experimental points and their fitting curve at $C = 3.3$ equiv/L, where $C = C_A + C_B$ and $y_A = n_A^*/n_T$.

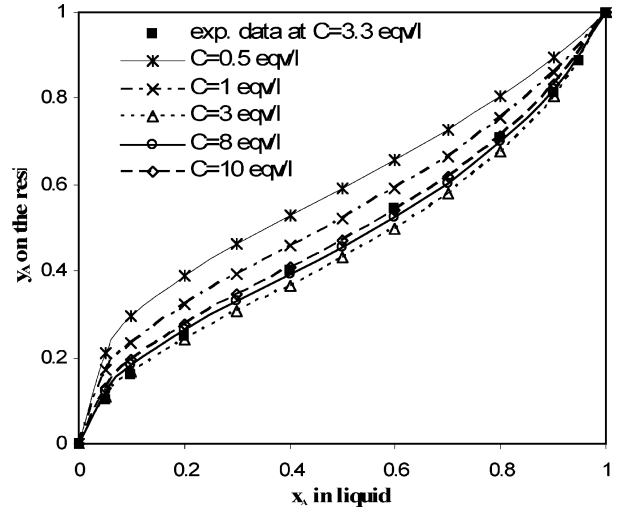

Figure 4. Equilibrium curves based on a thermodynamic equilibrium model, according to the total liquid concentration (C), where $C = C_A + C_B$ and $y_A = n_A^*/n_T$.

by an extended Debye−Hückel expression and those on the resin by the Wilson vapor−liquid equilibrium (VLE) model under the assumption of an analogy between solute−resin and vapor−liquid systems.[24] The thermodynamic equilibrium model predicts equilibrium concentrations of the three cation components (Ca^{2+}−H^+ and K^+) in the concentration range up to 12 N within an experimental error that is estimated to be 1%−2% of the total resin capacity.[23]

To determine the dependency of the equilibrium line on various liquid concentrations, the equilibrium lines are obtained based on the thermodynamic equilibrium model.[23] Figure 4 demonstrates that the equilibrium concentration of A (y_A), calculated by the thermodynamic model, varies slightly within 3 equiv/L $\leq C_{A+B} \leq$ 10 equiv/L. Although the thermodynamic equilibrium model provides more-reliable adsorption isotherms over the broad concentration range, eq 12 is used in this study because (i) simulation (e.g., model parameter estimation, sensitivity analysis, and optimization) with the thermodynamic equilibrium model requires a much longer computational time than eq 12, because of nonlinear iteration procedures in solving the thermodynamic model; (ii) the predictions from eq 12 are relatively good over the concentration range of interest (3.0 equiv/L $\leq C_{A+B} \leq$ 8.0 equiv/L, as shown in Figure 4; and (iii) there is no significant difference between simulation results with eq 12 and those with the thermodynamic equilibrium model, as observed in Tables 3 and 4.

4. In Situ Experiments, Simulation and Optimization Results

Mathematical models are required to be capable of representing experimental results as closely as possible. Section 3 presented a relatively simple SMB model. Therefore, the model should be validated by comparing the experimental data and the simulation results. After the model is validated and the simulation results are determined to agree with the experimental data, it can be used for the model-based optimization of operating conditions.

In this section, simulation results and in situ experiments are compared both for the pilot- and industrial-scale plants. Because of the uncertainty of the model parameters such as resin capacity, bed voidage, dispersion coefficient, mass-transfer coefficient, and adsorption isotherm, sensitivity analysis is performed for these parameters. Experimental and simulation procedures are presented in the following subsection.

4.1. Experimental and Simulation Procedures. The total of 16 tests were performed by experienced staff at the industrial company on the pilot plant configured as [2/5/2−1−1/4/1]. The tests were performed within the feasible operating region, changing the shifting time (or cycle time) and the two flow rates (V1 and FS). The 16 tests are composed of four different flow rates of V1 at three different cycle times (5, 6, and 7 min) and four different flow rates of FS at the 5-min cycle time, as shown in Table 5. Table 1 shows experimental conditions for one of the 16 tests (test P3 in Table 5). Only one test was performed in the industrial-scale plant configured by [3/3/3−1−1/4/1], as reported in Table 2.

The feed compositions of TS and TK changed only slightly, according to feed preparation, as shown in Tables 1 and 2. However, their fluctuations are small. During the cycle time, V1, V2, TS, and TK were injected with a constant flow rate and, at the same time, FS, KK, and SV were also withdrawn at a constant flow rate. KV was recycled to V1. The fresh V1 flow rate was (V1 − KV), because of the recycle flow.

Before each test was performed, all the columns were washed out and filled with fresh water. To reach a cyclic steady state, 3 rounds (48 shiftings) were operated under the same conditions. After the preloading, 1 round (16 shiftings) was performed for the data analysis. Thus, a total of 4 rounds (∼5 h) were run for each test. Each solution that was withdrawn at each shifting in the fourth round was collected in four tanks for each of FS, KK, SV, and KV. The four solutions were subsequently analyzed in the laboratory. As a result, the analyzed concentrations were averaged values over the last round.

For the key components (A for Ca^{2+}−H^+ and B for K^+), the purity and the dilution are determined from laboratory analysis:

$$\text{purity} = \frac{\bar{C}_{\text{B or A in FS or KK}}}{(\bar{C}_A + \bar{C}_B)_{\text{FS or KK}}} \tag{13}$$

$$\text{dilution} = 1 - \frac{(\bar{C}_A + \bar{C}_B)_{\text{FS or KK}}}{(\bar{C}_A + \bar{C}_B)_{\text{TS or TK}}} \tag{14}$$

where $\bar{C}_A$ or $\bar{C}_B$ represents the measured average concentration. A high purity of K^+ in the FS solution indicates a high-quality product. The purity of Ca^{2+}−H^+ in the KK solution indicates how much the Ca^{2+}−H^+ ions that were absorbed on the resin

Table 3. In Situ Experimental Data and Simulation Results for Average Liquid Concentrations, Purity and Dilution in the Industrial-Scale SMB Plant

	Concentration in FS				Concentration in KK			
	A (equiv/L)	B (equiv/L)	purity (%)	dilution (%)	A (equiv/L)	B (equiv/L)	purity (%)	dilution (%)
experimental data	2.23	3.74	62.7	42.2	1.59	0.20	88.8	53.9
simulation with eq 12	2.23	3.82	63.2	41.8	1.60	0.21	88.3	53.5
simulation with a thermodynamic equilibrium model	2.21	3.83	63.5	41.8	1.61	0.21	88.6	53.5

Table 4. In Situ Experimental Data and Simulation Results for Average Resin Concentrations and Resin Utility in the Industrial-Scale SMB Plant

	Resin of BW Column			Resin of V1 Column			
	A (equiv/L)	B (equiv/L)	% in K^+ ion form	A (equiv/L)	B (equiv/L)	% in K^+ ion form	resin utility[a] (%)
experimental data	0.67	2.46	78.6	2.79	0.37	11.7	66.9
simulation with eq 12	0.51	2.68	84.0	2.63	0.56	17.6	66.4
simulation with a thermodynamic equilibrium model	0.43	2.76	86.7	2.57	0.62	19.5	67.2

[a] Resin utility = $(\%\text{ in } K^+\text{ ion form})_{\text{BW column}} - (\%\text{ in K ion form})_{\text{V1 column}}$.

Table 5. Experimental Task Matrix in the Pilot Plant[a]

		Production Section				Regeneration Section			
test	cycle time (s)	V1 L/cycle	TS L/cycle	FS L/cycle	SV L/cycle	V2 L/cycle	TK L/cycle	KK L/cycle	KV L/cycle
P1	300	13.0	2.1	5.6	9.5	11.3	3.8	8.8	6.3
P2	300	11.4	2.1	5.6	7.9	11.3	3.8	8.8	6.3
P3	300	10.7	2.1	5.6	7.2	11.3	3.8	8.8	6.3
P4	300	10.0	2.1	5.6	6.5	11.3	3.8	8.8	6.3
P5	360	13.0	2.5	6	9.5	11.3	4.3	8.8	6.8
P6	360	11.4	2.5	6	7.9	11.3	4.3	8.8	6.8
P7	360	10.7	2.5	6	7.2	11.3	4.3	8.8	6.8
P8	360	10.0	2.5	6	6.5	11.3	4.3	8.8	6.8
P9	420	13.0	2.9	6.4	9.5	11.3	4.8	9.3	6.8
P10	420	11.4	2.9	6.4	7.9	11.3	4.8	9.3	6.8
P11	420	10.7	2.9	6.4	7.2	11.3	4.8	9.3	6.8
P12	420	10.0	2.9	6.4	6.5	11.3	4.8	9.3	6.8
P13	300	10.7	2.1	5.1	6.2	11.3	3.8	8.3	6.8
P14	300	10.7	2.1	5.6	6.7	11.3	3.8	8.3	6.8
P15	300	10.7	2.1	6.1	7.2	11.3	3.8	8.3	6.8
P16	300	10.7	2.1	6.6	7.7	11.3	3.8	8.3	6.8

[a] Reference: Kemira A/S internal report.

Table 6. Sensitivity and Elasticity of Model Parameters on Purity, Dilution in the FS Solution, and Resin Utility

	n_T	$\epsilon_{b,eff}$	k_{prod}	k_{regen}	D_{ax}/v_L
nominal value	2.0	0.5527	0.4	0.7	0.04
minimum value	1.9	0.5327	0.38	0.65	0.004
maximum value	2.1	0.5727	0.42	0.75	0.4
perturbation (%)	±5.0	±3.6	±5.0	±7.1	±1000
			Sensitivity (Elasticity)[a]		
purity in FS	10 (0.32)	−40 (−0.35)	17.5 (0.11)	5 (0.05)	−7.5 (−0.02)
dilution in FS	0 (0)	0 (0)	0 (0)	0 (0)	2.5 (0.002)
resin utility	−25 (−0.75)	98 (0.81)	17 (0.10)	6.2 (0.06)	−56.5 (−0.03)

[a] Elasticity values given in parentheses. Sensitivity $=(dy/dx)|_{x=\text{nominal value}}$, where x is the model parameters and y is the purity, dilution, or resin utility. Elasticity $= (d(\ln y)/d(\ln x))|_{x=\text{nominal value}} = (dy/y)/(dx/x)|_{x=\text{nominal value}}$.

are desorbed in the regeneration section. Thus, the higher the purity in the KK solution, the higher the purity in the FS solution. The dilution indicates a loss of all valuable ions such as NPK in ion form, i.e., NO_3^-, PO_4^{3-}, and K^+.

Two samples of resin particles of the regenerated resin (BW column) and the exhausted resin (V1 column) are also analyzed in the laboratory, after finishing a test at the three cycle times (5, 6, and 7 min). Thus, the solid concentration of the resin is also an average value for the two columns.

Simulation is performed for 15 columns, i.e., excluding one BW column, during 53 shiftings. The simulation parameters are also shown in Tables 1 and 2. For the sensitivity analysis of the five model parameters (see Table 6), at least 10 runs should be performed. In the simulations, concentration profiles exhibit steep moving fronts in several places, as will be shown later in Figure 6. Thus, a fast and accurate numerical scheme is desirable to solve the SMB model (eqs 2−5).[14] The non-iterative space−time CE/SE method[14,25] is used to solve the conservation laws represented by the PDEs in eq 2 for each column.

At the beginning of the first shifting (i.e., $t = 0$), the liquid concentration of all components is initialized to zero for all columns. The resin is initially set to 75% K^+ form and 25% $Ca^{2+}-H^+$ form for all columns:

$$C_A(0,z_{i,k}) = C_B(0,z_{i,k}) = 0 \quad (\text{for } i = 1, ..., N_m,\ k = 1, ..., 15) \quad (15a)$$

$$n_A(0,z_{i,k}) = 0.25n_T,\ n_B(0,z_{i,k}) = 0.75n_T \quad (\text{for } i = 1, ..., N_m,\ k = 1, ..., 15) \quad (15b)$$

where N_m is the number of meshes per column and n_T is the resin capacity. The assumption in eq 15b is somewhat unrealistic, because the initial resin concentration profile is dependent on the previous run and is not uniform (see Figure 7 presented later in this work). However, eq 15b is adopted because of the lack of information on the initial resin concentration. The effect of the unrealistic initial condition is negligible after 2 rounds of simulation. Each run is completed after 53 shiftings (3.5 rounds for 15 columns).

All simulations were performed on a personal computer (PC) that was equipped with a single 1.3 GHz processor. The number of mesh points per column is assumed to be $N_m = 26$ for all the cases, and the number of time steps per cycle time is $N_t = 71$. As a result, the CFL number $\nu \equiv v_L \Delta t/\Delta z \approx 0.6$, where $\Delta t = \tau/(N_t - 1)$ and $\Delta z = L_{c,eff}/(N_m - 1)$. The computational time is <1 min for each run. The effects of the number of mesh points and the CFL number are not expected to be significant, because, for the NPK fertilizer process, the Peclet number is not large ($Pe = 65-105$) and the Stanton number is small ($St = 1.4-5.7$) (see Tables 1 and 2).[14]

In the simulation, the average liquid concentrations in the FS and KK solutions are obtained from the numerical integration[29] of liquid concentrations at the exit of FS and KK columns over the last shifting (i.e., the 53rd shifting):

$$\bar{C}_{k,53\text{rd shifting}} = \frac{\sum_{i=1}^{N_t} C_{k,i}\Delta t}{\tau} \qquad (\text{for } k = \text{A or B}) \qquad (16)$$

where N_t is the number of time steps. The average resin concentrations are also based on the values at the end of the last shifting. The 10th column and the 1st column are used for the regenerated resin (BW column in the experiment) and the exhausted resin (V1 column in the experiment) analyses, respectively. The average resin concentrations for each component are obtained as follows:

$$\bar{n}_{k,53\text{rd shifting}} = \frac{\sum_{i=1}^{N_m} n_{k,i}\Delta z}{L_{c,eff}} \qquad (\text{for } k = \text{A or B}) \qquad (17)$$

In Tables 3 and 4, the two average concentrations ($\bar{C}$ and $\bar{n}$) obtained from experiments and simulations are reported for the industrial-scale plant. The model parameters mentioned in section 3 were estimated and confirmed on the basis of the 16 pilot-plant experiments, which is essential for model-based simulation and optimization.

4.2. Results from the Pilot Plant. Simulation results performed under the operating conditions shown in Table 1 and recently have been illustrated in Lim and Lee.[19] The maximum deviation between the simulation and the experiment remains within ~10% in absolute deviation for the purity of 16 pilot-plant experiments. The trends of the purity variations also exhibit good agreement for all the cycle times.[19]

It is important to notice that this six-zone SMB process is operated at a relatively low purity (60%−70%; see Table 3) of the product solution, because the amounts of valuable NO_3^- and PO_4^{3-} in the dilution stream also increase when the process is operated at a higher potassium purity.

In Figure 5, the operating conditions of the 16 experimental tests are plotted in the space of m_2-m_5, where m_2 is the zone II fluid-to-solid flow-rate ratio ($m_2 = Q_2/Q_s$) and m_5 is the zone V fluid-to-solid flow-rate ratio ($m_5 = Q_5/Q_s$). Here, the most important zones (zones II and V) in this two-section SMB process are analyzed within the *m*-plane (i.e., the fluid-to-solid flow-rate ratio plane), such as the Triangle theory,[26] which was developed based on equilibrium adsorption and linear or Langmuir isotherms for the TMB operation. Tests 1−4, 5−8, and 9−12 are performed by changing m_2 at a constant m_5. The purity shows a tendency to decrease as the operation moves away from the diagonal line in Figure 5.[19] Tests 13−16 are conducted at constant m_2 and m_5. The previously reported experimental and calculated purity trends are compatible with the Triangle theory. However, the separation performances (purity, productivity, and desorbent consumption) of this SMB unit are not straightforwardly optimized by the Triangle theory, because adsorption isotherms are strongly nonlinear and the process is operated in a nontraditional way. This will be further explored below after discussing results from the industrial plant.

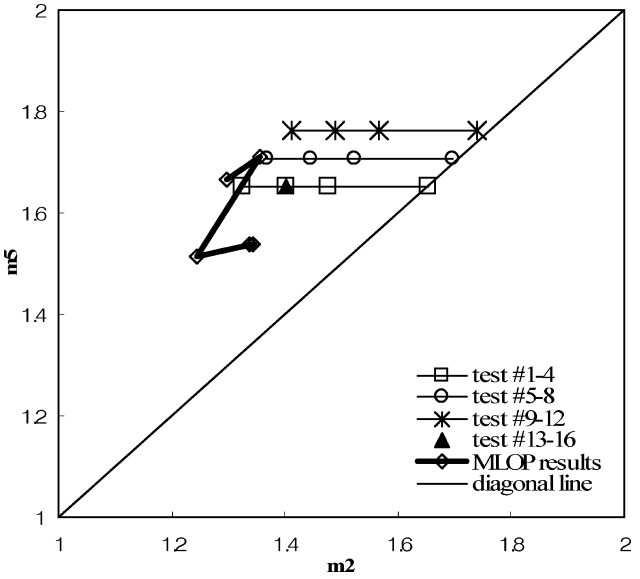

Figure 5. Flow-rate ratio analysis of zones II and V for 16 experimental tests in a pilot plant and model-based optimization results in an industrial plant.

4.3. Results from the Industrial Plant. One experiment is conducted in the industrial plant under the experimental (and simulation) conditions given in Table 2. It is observed that the experimental average liquid concentrations ($\bar{C}_j$) during the entire fourth round (i.e., shiftings 46−60) are in good agreement with the simulation results, within a 3% error bound (see Table 3).

Table 3 reports the average concentrations, purity, and dilution in the FS and KK solutions at the final shifting. To investigate the effects of the adsorption isotherm model on the process performance, two simulations with the two-component model in eq 12 and with the three-component model[23] are performed. The two simulation results are in good agreement, as shown in Tables 3 and 4. Table 4 summarizes the in situ experimental and simulation results of solid concentrations in the BW column (or regenerated resin) and V1 column (or exhausted resin). Some differences between experiments and simulations are observed in the average resin concentrations. However, the resin utility of the simulation agrees well with that of the experiment. In Tables 3 and 4, it is demonstrated that the polynomial adsorption isotherms (eq 12) fitted to experimental points represent the rigorous three-component model[23] well. Note, in Tables 3 and 4, that the concentrations of component A, which are obtained from the three-component-based thermodynamic model,[23] are the sum of those of the two components, Ca^{2+} and H^+.

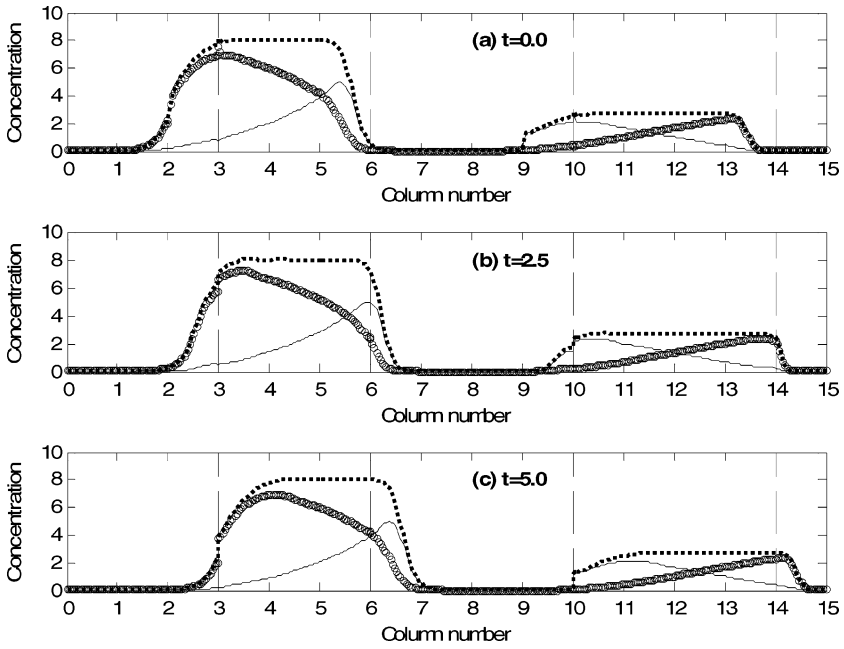

Figure 6. Liquid concentration distribution of $Ca^{2+}-H^{+}$ ions (circles), K^{+} ions (solid line), and total concentration (dotted line) over 15 columns at three different times within one cycle ($\nu = 0.6$, $N_m = 26$).

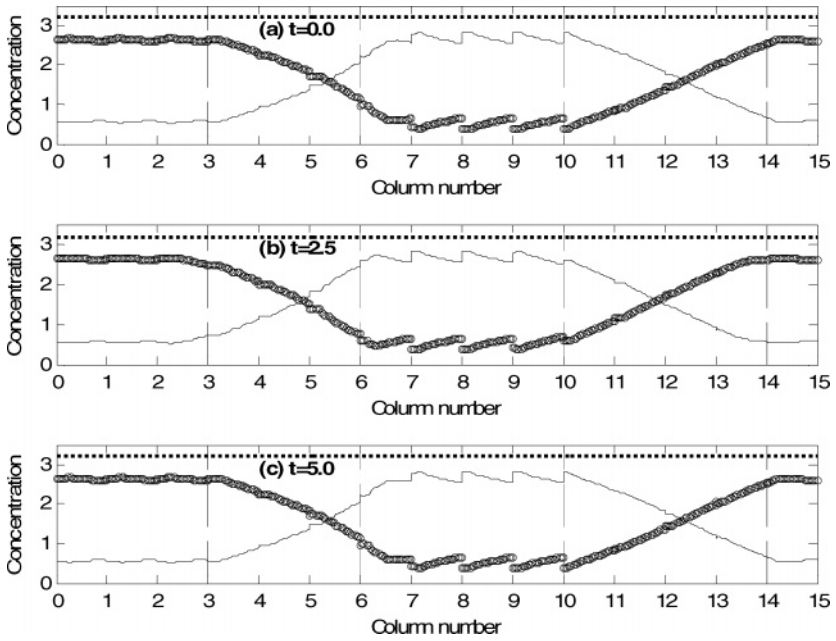

Figure 7. Solid concentration distribution of $Ca^{2+}-H^{+}$ ions (circles), K^{+} ions (solid line), and total concentration (dotted line) over 15 columns at three different times within one cycle ($\nu = 0.6$, $N_m = 26$).

For the final shifting (the 53rd shifting), the liquid and solid concentrations of $Ca^{2+}-H^{+}$ and K^{+} are illustrated, along with the column number, in Figures 6 and 7, respectively, at three different times during the 5-min cycle. At the beginning of the cycle ($t = 0$), TS and TK are fed at $z = 3$ and $z = 10$, respectively, whereas FS and KK begin to be withdrawn at $z = 6$ and $z = 14$, respectively. The four positions ($z = 3$, 6, 10, and 14) are depicted as the dashed lines in Figures 6 and 7. The total concentrations at each axial position are shown as the bold dotted line. Slight overshoots that are caused by the feed are observed at the feed points ($z = 3$ and $z = 10$) in Figure 6a. Discontinuous concentrations at $z = 2$ and $z = 9$ (inlet points of the 3rd and 10th column) in Figure 6a originate from the concentrations at the feed points ($z = 3$ and $z = 10$) of the previous cycle. The $Ca^{2+}-H^{+}$ concentration at the FS port ($z = 6$) is effectively zero and the K^{+} concentration is low (i.e., high purity and low concentration of K^{+}), because of the one-column advanced operation.

At the middle of the cycle in Figure 6b, a maximum point of the K^{+} concentration is reached at $z = 6$ and that of the $Ca^{2+}-H^{+}$ at $z = 14$. Figure 6c shows concentration profiles at the end of the cycle ($t = 5$ min). These dynamic behaviors during one cycle represent the cyclic stationary state, which is repeated over the next cycle. Note that the concentration dynamics shown in Figures 6 and 11 (presented later in this work) cannot be obtained from the TMB[3,4] or CMB[5,6] models. Indeed, the TMB or CMB models provide just one steady-state concentration profile along the columns. For nonlinear adsorption isotherms, the profile of the TMB models can be quite different from that of the SMB models at the middle of the cycle time, which demonstrates that SMB processes must be described by rigorous dynamic models such as the SMB model (see eqs 2−5).[27]

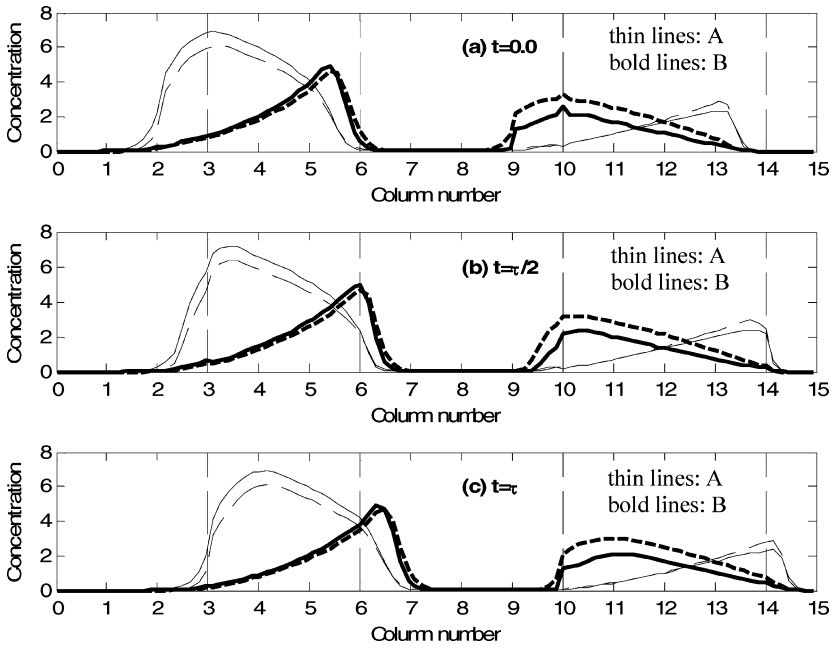

Figure 8. Comparison of SMB simulation results for the liquid phase at level 2 (solid lines) and level 4 repeated (dashed lines) at three different times within the 53rd shifting.

The cyclic stationary state is shown for resin concentration distributions over the columns in Figure 7. Because of the counter-current-like flow of the SMB operation, the regenerated resin passing the seventh column (6 min $\leq z \leq$ 7 min) contacts with the reactive solution at the sixth column (5 min $\leq z \leq$ 6 min). The exhausted resin is found at the first column (0 min $\leq z \leq$ 1 min). The resin concentration profiles give important information on the resin performance and design, because the process performance is directly related to resin utility in Figure 8. The total liquid concentration is globally constant over production zone II (3 min $\leq z \leq$ 6 min) and the regeneration zone V (10 min $\leq$ z $\leq$ 14 min) in Figure 6 (b). The total concentration in the solid phase is equal to the resin capacity everywhere in Figure 7. Thus, the electroneutrality condition in eq 11a and eq 12 is satisfied both in the liquid and solid phases.

Note that inactive regions (or nonadsorption regions because of equilibrium ($C_A + C_B$) $\approx$ 0) are found in many places (see Figure 6) where the resin is saturated with $Ca^{2+}-H^{+}-K^{+}$ ions (see Figure 7). The equilibrium correlation (eq 12a) is valid only for($C_A + C_B$) $\neq$ 0. If eq 2 is used for all regions instead of eq 10 or eq 11, a virtual desorption could occur in these inactive regions to satisfy the electroneutrality condition, as mentioned in section 3.4. Therefore, unphysical numerical results (e.g., negative concentrations) can be obtained using the traditional LDF model (eq 2b). Besides, eq 12 is infeasible if negative concentrations appear. As a result, it is necessary to use the generalized LDF model (eq 12) for this ion-exclusion and ion-exchange chromatographic system. This generalized LDF model implies the thermodynamic insight that there is no apparent adsorption/desorption flux when ($C_A + C_B$) = 0, because of equilibrium between the liquid and solid phases.

The industrial-scale plant with these operating conditions does not seem to be fully exploited, because the inactive regions, e.g., zone I (0 min $\leq z \leq$ 1 min) and zone III (7 min $\leq z \leq$ 9 min), are too long, as shown in Figure 6. Therefore, it is relevant to investigate the potential benefit from optimizing the operating conditions. Such a study on the industrial-scale process is presented below.

4.4. Optimization Results for the Industrial-Scale Process. Model-based optimization is performed for the industrial-scale six-zone SMB process (see Table 2). The objective of the optimization problem is to minimize wash-water consumption, while maintaining a maximum productivity at the given purity level. An optimization procedure (multilevel optimization procedure, MLOP) for this objective has been presented in the work by Lim.[30] The four-level MLOP optimization approach may be briefly summarized as follows:

- Level 1: initialization based on a standing wave analysis,[5] under the assumption of linear adsorption isotherms.
- Level 2: TMB optimization, using nonlinear adsorption isotherms and nonequilibrium design.
- Level 3: SMB optimization, for maximization of productivity.
- Level 4: SMB optimization, for minimization of desorbent consumption.
- If the procedure has converged close to a constant cycle time, it is terminated; else, go to level 3.

Because the operating conditions shown in Table 2 are well-adjusted through a company procedure, the optimization with MLOP[30] starts at level 3. The optimization variables are the six flow rates (Q_{V1}, Q_{TS}, Q_{FS}, Q_{V2}, Q_{TK}, and Q_{KK}) and the cycle time (τ). Because Q_{V1} includes the recycle flow rate (Q_{KV}), the net wash-water flow rate at $z = 0$ is assigned as follows:

$$Q_{V1_{net}} = Q_{V1} - Q_{KV} \tag{18}$$

In the optimization problems, Q_{V1} is replaced by the new variable $Q_{V1_{net}}$. The objective function and the constraints at level 3 are specified:

$$\underset{x}{\text{Max}} \left[\text{Prod} = \frac{Q_{FS}\bar{C}_{FS,B}}{N_c(1-\epsilon_b)V_c} \right] \quad (\text{for } x = Q_{TS}, Q_{FS}, Q_{TK}, \text{and } Q_{KK}) \tag{19}$$

subject to

$$0.65 \le y_1 = \mathrm{Pur}_{\mathrm{FS,B}} \le 1.0 \tag{20a}$$

$$0.85 \le y_2 = \mathrm{Pur}_{\mathrm{KK,A}} \le 1.0 \tag{20b}$$

$$y_3 = \mathrm{Dilut}_{\mathrm{FS}} \le 0.45 \tag{20c}$$

$$y_4 = \mathrm{Dilut}_{\mathrm{KK}} \le 0.55 \tag{20d}$$

$$y_5 = Q_{\max} \le 1.75 \tag{20e}$$

where

$$\bar{C}_{\mathrm{FS,B}} = \frac{\sum_{i=1}^{N_t} C_{\mathrm{B},i}\Delta t}{\tau} \qquad (\text{at } N_{\mathrm{shift}} = 53) \tag{21a}$$

$$\mathrm{Pur}_{\mathrm{FS,B}} = \frac{\bar{C}_{\mathrm{B\ in\ FS}}}{(\bar{C}_{\mathrm{A}} + \bar{C}_{\mathrm{B}})_{\mathrm{FS}}} \tag{21b}$$

$$\mathrm{Pur}_{\mathrm{KK,A}} = \frac{\bar{C}_{\mathrm{A\ in\ KK}}}{(\bar{C}_{\mathrm{A}} + \bar{C}_{\mathrm{B}})_{\mathrm{KK}}} \tag{21c}$$

$$\mathrm{Dilut}_{\mathrm{FS}} = 1 - \frac{(\bar{C}_{\mathrm{A}} + \bar{C}_{\mathrm{B}})_{\mathrm{FS}}}{(\bar{C}_{\mathrm{A}} + \bar{C}_{\mathrm{B}})_{\mathrm{TS}}} \tag{21d}$$

$$\mathrm{Dilut}_{\mathrm{KK}} = 1 - \frac{(\bar{C}_{\mathrm{A}} + \bar{C}_{\mathrm{B}})_{\mathrm{KK}}}{(\bar{C}_{\mathrm{A}} + \bar{C}_{\mathrm{B}})_{\mathrm{TK}}} \tag{21e}$$

In eq 21a, $\bar{C}_{\mathrm{FS,B}}$ is the average concentration of B during the final shifting ($N_{\mathrm{shift}} = 53$). In eqs 21d and 21e, the dilution indicates a loss of all valuable ions, such as NPK in the ion form, i.e., NO_3^-, PO_4^{3-}, and K^+ , as previously stated. Note that the process is operated at relatively low purity to reduce the loss of NO_3^-, PO_4^{3-}, and K^+, as mentioned previously. The two wash-water flow rates ($Q_{\mathrm{V1_{net}}}$ and Q_{V2}) and the cycle time (τ) are maintained constant at this level.

The objective function and the constraints at level 4 are given as follows:

$$\min_x \lfloor Q_{\mathrm{des}} = Q_{\mathrm{V1_{net}}} + Q_{\mathrm{V2}} \rfloor \quad (\text{for } x = Q_{\mathrm{V1_{net}}}, Q_{\mathrm{V2}}, \tau) \tag{22}$$

subject to

$$0.65 \le y_1 = \mathrm{Pur}_{\mathrm{FS,B}} \le 1.0 \tag{23a}$$

$$0.85 \le y_2 = \mathrm{Pur}_{\mathrm{KK,A}} \le 1.0 \tag{23b}$$

$$y_3 = \mathrm{Dilut}_{\mathrm{FS}} \le 0.45 \tag{23c}$$

$$y_4 = \mathrm{Dilut}_{\mathrm{KK}} \le 0.55 \tag{23d}$$

$$y_5 = Q_{\max} \le 1.75 \tag{23e}$$

$$29.1 \le y_6 = \mathrm{Prod} \tag{23f}$$

where productivity in the production section (Prod) is defined as follows:

$$\mathrm{Prod} = \frac{Q_{\mathrm{FS}}\bar{C}_{\mathrm{FS,B}}}{N_{\mathrm{c}}(1 - \epsilon_{\mathrm{b}})V_{\mathrm{c}}} \tag{24}$$

Note that the minimum value of productivity in eq 23f is obtained from the optimization results of level 3.

Table 7 reports the MLOP results for the NPK ion-exchange SMB process. The operating conditions and simulation results corresponding to levels 1 and 2 are referenced in Tables 2 and 3. Levels 3 and 4 are repeated once, to ensure a converged optimum solution. The values of m_2 and m_5 at each level are also shown in Table 7.

At level 3 and level 3 repeated, higher productivities are achieved by increasing Q_{TS} and Q_{FS}, and by increasing Q_{TK}, decreasing Q_{KK}, and increasing Q_{KV} (or the recycle flow rate). Because Q_{FS} should increase to augment the productivity in eq 24, Q_{TS} and Q_{FS} also increase. As shown in the m_2-m_5 plane (see Figure 5), m_5 decreases at a similar m_2 value ($m_2 = 1.35$) to increase productivity. Decreasing m_5 results in an increase in the residence time in the regeneration section, which leads to a higher regeneration ratio of the resin (also see Figures 8 and 9).

At level 4 and level 4 repeated, the desorbent consumption is reduced by adjusting the cycle time, while the productivity is maintained. In this case, m_2 increases at a similar m_5 value ($m_5 = 1.52$) to decrease the wash-water consumption (see Figure 5). Increasing m_2 results in a decrease in the residence time in the production section. Nevertheless, productivity remains high by maintaining a high regeneration ratio of the resin (see Table 7).

The optimization result is that wash-water consumption is reduced by 5.4% ($Q_{\mathrm{des}} = 1.454 \rightarrow 1.375$) at a 5% higher productivity (Prod $= 28.23 \rightarrow 29.65$), compared to the normal operating condition at levels 1 and 2.

Figures 8 and 9 compare concentration distributions over the columns in the liquid and solid phases, respectively. The thin lines indicate component A ($Ca^{2+} + H^+$) and the bold lines component B (K^+). Concentration profiles are shown at three different times within the 53rd shifting period, i.e., at the beginning ($t = 0$), the middle ($t = 2/\tau$), and the end ($t = \tau$) of the 53rd cycle.

Figure 8 shows that the concentration profiles of A and B are reduced in the production section, whereas those of A and B are increased in the regeneration section. In Figure 9, the resin is regenerated much more by K^+ (or B) at the optimized flow rates and cycle time than under the normal operating condition. This regenerated resin results in a high driving force in the production section, higher productivity, and lower desorbent consumption.

4.5. Sensitivity Analysis of Model Parameters. The sensitivity analysis is presented only for the industrial-scale plant. Table 6 shows nominal values and perturbations of the five model parameters: the resin capacity (n_{T}), the effective bed voidage ($\epsilon_{\mathrm{b,eff}}$), the mass-transfer coefficients in the production section (k_{prod}) and in the regeneration section (k_{regen}), and the axial dispersion coefficient (D_{ax}).

The resin capacity n_{T} and the effective bed voidage $\epsilon_{\mathrm{b,eff}}$ were determined through experiments by the industrial collaborator. Thus, their perturbations can be considered as potential extreme experimental errors. The mass-transfer coefficients k_{prod} and k_{regen} and the axial dispersion coefficient D_{ax} were initialized from empirical correlations, as explained in section 3, and were identified by comparing the simulation results and the experimental data from the pilot plant. The effect of $D_{\mathrm{ax}}/v_{\mathrm{L}}$ on the process performance is small; therefore, a large perturbation ($\pm 1000\%$) is used.

The sensitivity (dy/dx) of the process performance (y) has the same units as the model parameters (x). However, the elasticity ($(dy/dx) \times (x/y)$) is dimensionless and, therefore, is most useful to reveal which parameters most strongly influence the process performance. Table 6 reports the sensitivity and elasticity of purity and dilution in the FS solution, as well as resin utility, according to the five model parameters (elasticity

Table 7. Results of the Multilevel Operating Procedure (MLOP) for the NPK Ion-Exchange SMB Process

	Variables									Simulation Results			Objective Functions	
	$Q_{V1_{net}}$ (m^3/min)	Q_{TS} (m^3/min)	Q_{FS} (m^3/min)	Q_{V2} (m^3/min)	Q_{TK} (m^3/min)	Q_{KK} (m^3/min)	m_2	m_5	τ (min)	Pur_{FS} (%)	$Prod_{FS}$	Q_{max}[a]	Prod[b]	Q_{des}[c]
levels 1 and 2	0.388	0.234	0.406	1.066	0.440	0.954	1.30	1.67	5.00	63.2	28.23	1.51	28.23	1.454
level 3	0.388	0.236	0.409	1.066	0.481	0.944	1.36	1.71	5.00	65.0	29.19	1.547	29.19	1.454
level 4	0.458	0.236	0.409	0.923	0.481	0.944	1.24	1.51	4.87	65.0	29.12	1.40	29.12	1.381
level 3, repeated	0.458	0.239	0.428	0.923	0.505	0.879	1.34	1.54	4.87	65.0	29.68	1.43	29.68	1.381
level 4, repeated	0.456	0.239	0.428	0.919	0.505	0.879	1.34	1.54	4.88	65.0	29.64	1.42	29.65	1.375

[a] $Q_{max} = \max [(Q_{V1} + Q_{TS}),(Q_{V2} + Q_{TK})]$. [b] Productivity has units of mol min^{-1} m^{-3}, based on the total resin volume ($V_S = (1 - \epsilon_b)L_cSN_c$). [c] $Q_{des} = Q_{V1_{net}} + Q_{V2}$.

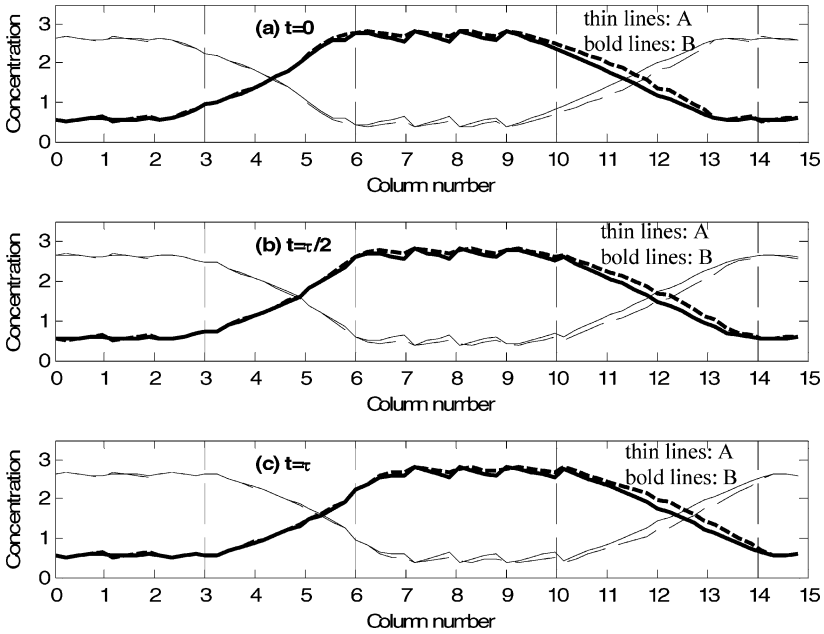

Figure 9. Comparison of SMB simulation results for the solid phase at level 2 (solid lines) and level 4 repeated (dashed lines) at three different times within the 53rd shifting.

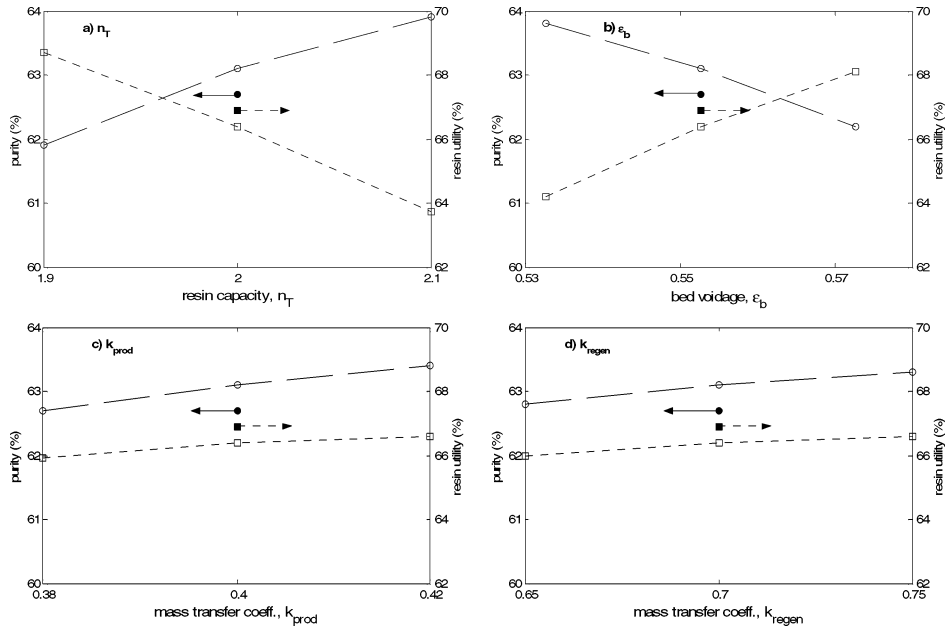

Figure 10. Variation of purity in FS (circles) and resin utility (squares) with model parameters (filled circles and filled squares are experimental points).

is shown in parentheses in this table). The resin capacity (n_T) and the bed voidage ($\epsilon_{b,eff}$) affect the purity and the resin utility relatively strongly, as indicated by their elasticity values. As a result, n_T and $\epsilon_{b,eff}$ should be accurately measured by the experiments.

Figure 10 depicts variations of the purity and the resin utility, with respect to four model parameters. Experimental data are marked in the figure by filled circles and squares. Note that the purity is positively dependent on the resin capacity (n_T), because a higher n_T implies a higher driving force. However, the resin

utility is reduced as n_T increases. In contrast, these relationships are reversed for the bed voidage (see Figures 10a and 10b). As $\epsilon_{b,eff}$ increases, the interstitial fluid velocity (v_L) decreases and the ratio of the resin volume to the fluid volume (i.e., $(1 - \epsilon_{b,eff})/\epsilon_{b,eff}$ in eq 2a) also decreases. The former relation results in an increase in the resin utility, because of the increase of the fluid residence time, whereas the latter relationship decreases the purity, because of a reduced resin volume.

A high mass-transfer coefficient means a high adsorption or desorption rate. Therefore, the purity and the resin utility increase as k_{prod} and k_{regen} increase, where the effect of k_{prod} on the purity and the resin utility is approximately twice that of k_{regen} (see elasticity values given in parentheses in Table 6). Changes of 10% in k_{prod} result in 1.1% changes in the FS purity and 10% changes in k_{regen} result in 0.5% changes in the FS purity.

A low axial dispersion coefficient enhances the process performance on the purity and resin utility, although the static effect is small. All five model parameters have minor effects on the dilution in the FS solution, because the dilution is defined as a loss of total ions in eq 14.

Through this sensitivity analysis, the effects of model parameters on the process performance are identified and it is demonstrated that the process performance can be enhanced by adjusting the operational conditions to achieve higher k values and lower D_{ax} values.

5. Conclusions

To perform one experimental test of the nitrogen−phosphorus−potassium (NPK) ion-exchange simulated-moving-bed (SMB) process, ~5 h are required to reach a cyclic stationary state. To determine the optimum operation conditions for the cycle time and flow rates in a given column configuration, many experimental runs must be performed. Thus, several months may be needed to determine near-optimum operation conditions through experiments.

The nonequilibrium SMB chromatographic model used is characterized by a spatially distributed dynamic system for several columns. An explicit time-marching scheme, i.e., the so-called conservation element and solution element (CE/SE) method, is used to solve the distributed model described by partial differential equations (PDEs) accurately and effectively. The CE/SE method enables accurate and efficient tracking of steep concentration profiles moving along the column axis. Thereby, simulation, parameter estimation, and optimization studies can be accelerated. When using conventional linear driving force (LDF) models for nonequilibrium adsorption, an unphysical desorption can occur in nonadsorption (or inactive) regions of the column, where an equilibrium state between the liquid and solid phases may exist. The inactive regions appear during operation for the ion-exchange SMB process, because of the wash-water zones, which are included to ensure ion exclusion. A generalized LDF adsorption rate model is used to enable switching between equilibrium and nonequilibrium adsorption models. It is demonstrated that the switching functions enables us to satisfy the electroneutrality condition in ion-exchange chromatography.

In the simulation study on the six-zone SMB process, <1 min is needed to obtain the cyclic stationary state (i.e., $\sim 1/300$ of the experimental time, using the CE/SE method). Model parameters (e.g., mass-transfer coefficients in production and regeneration sections) are estimated by comparing simulation results with the experimental data. The effects of the model parameters on the process performance are examined through sensitivity analysis. The obtained model results are compared favorably both to pilot- and industrial-scale data.

Through application of the multilevel optimization procedure (MLOP) to NPK ion-exchange SMB chromatography, it is shown that wash-water consumption can be reduced, while also achieving a higher productivity. It is also observed that desorbent consumption can be reduced near the same productivity value by adjusting the shifting time, thereby also reducing the energy consumption in downstream evaporators.

Acknowledgment

This research was financially supported by the Danish Energy Authority, through Grant Nos. ENS 1223/99-0008 and ENS 1273/00-0026. The authors appreciate the advice from Dr. Sin-Chung Chang on the application of the space-time CE/SE method to the packed-bed chromatographic model. The authors thank the Innovation Department of Kemira Denmark A/S for helpful discussions and providing experimental data. This work is also financially supported by the Korea Research Foundation (KRF) Grant funded by the Korean Government (MOEHRD), through Project No. KRF-2005-D00108.

Nomenclature

C = concentration in fluid phase (equiv/L on a liquid volume basis)
$\bar{C}$ = average liquid concentration (equiv/L on a liquid volume basis)
C_{in} = inlet concentration of fluid at $z = 0$ (equiv/L on liquid volume basis)
D_{ax} = axial dispersion coefficient (m^2/min)
D_c = column inner diameter (m)
$g(C)$ = adsorption isotherm function in eq 2c
k = overall adsorption rate coefficient (min^{-1})
k_f = liquid film mass-transfer coefficient (m/min)
k_{prod} = mass-transfer coefficient in the production section (m/min)
k_{regen} = mass-transfer coefficient in the regeneration section (m/min)
L_c = column length (m)
$L_{c,eff}$ = effective column length (m)
m_2 = zone II fluid-to-solid flow-rate ratio; $m_2 = Q_2/Q_s$
m_5 = zone V fluid-to-solid flow-rate ratio; $m_5 = Q_5/Q_s$
n = concentration in resin or solid phase (equiv/L on a particle volume basis)
n^* = equilibrium concentration in resin or solid phase (equiv/L on a particle volume basis)
$\bar{n}$ = average solid concentration (equiv/L on a particle volume basis)
N_m = number of mesh points per column
N_{shift} = number of shiftings
n_T = resin capacity (equiv/L on a bed volume basis)
$n_{T,p}$ = resin capacity (equiv/L on a particle volume basis)
N_t = number of time steps per cycle time
Pe = Peclet number; $Pe = v_L L_{c,eff}/D_{ax}$ or $Pe = v_L d_p/D_L$
Q = flow rate (m^3/min)
Q_2 = flow rate of zone II (m^3/min)
Q_5 = flow rate of zone V (m^3/min)
Q_{in} = inlet flow rate of fluid at $z = 0$ (m^3/min)
Q_s = flow rate of solid particles; $Q_s = (1 - \epsilon_{b,eff})SL_{c,eff}/\tau$ (m^3/min)
r_i = adsorption rate (equiv/L/min)
$r_i^{general}$ = generalized adsorption rate (equiv/L/min)
S = cross-section area of column (m^2)
St = Stanton number; $St = kL_{c,eff}/v_L$

t = time (min)
T = temperature (°C)
V_{dead} = dead volume (m^3)
v_L = interstitial fluid velocity (m/min)
V_{liquid} = liquid volume (m^3)
V_{total} = sum of dead volume and liquid volume (m^3)
x_A = mole fraction of $C_{Ca^{2+}-H^+}$ to total liquid concentration
y_A = mole fraction of $n^*_{Ca^{2+}-H^+}$ to total solid concentration
z = axial direction of column (m)

Greek Letters

α = logical variables in the node model, eq 5
ϵ_b = interstitial bed voidage
$\epsilon_{b,eff}$ = effective interstitial bed voidage
ϕ_{sum} = sum kernel in eq 11
$\phi_{product}$ = product kernel in eq 11
ν = CFL number
τ = cycle time or shifting time
Δt = uniform time step size (min)
Δz = uniform spatial step size (m)

Abbreviations

AE = algebraic equation
BC = boundary condition
CE/SE = conservation element/solution element
CMB = continuous moving bed
DAE = differential algebraic equation
IC = initial condition
LDF = linear driving force
NPK = nitrogen-phosphate-potassium
ODE = ordinary differential equation
PDAE = partial differential algebraic equation
PDE = partial differential equation
SMB = simulated moving bed
TMB = true moving bed

Literature Cited

(1) Klatt, K.-U.; Dünnebier, G.; Hanisch, F.; Engell, S. Optimal Operation and Control of Simulated Moving Bed Chromatography: A Model-based Approach. In *Chemical Process Control VI*, CACHE/AIChE Conference, Tucson, AZ, 2001; Rawlings, J. B., Ogunnaike, B.A., Eaton, J. W., Eds.; AIChE Symposium Series, Vol. 98, No. 326; Computer Aids for Chemical Engineering (CACHE) Publications: New York, 2002; p 239.

(2) Proll, T.; Kusters, E. Optimization Strategy for Simulated Moving Bed Systems. *J. Chromatogr., A* **1998**, *800*, 135.

(3) Ching, C. B.; Chu, K. H.; Hidajat, K.; Uddin, M. S. Experimental and Modeling Studies on the Transient Behavior of a Simulated Countercurrent Adsorber. *J. Chem. Eng. Jpn.* **1991**, *24* (5), 614.

(4) Beste, Y. A.; Lisso, M.; Wozny, G.; Arlt, W. Optimization of Simulated Moving Bed Plants with Low Efficient Stationary Phases: Separation of Fructose and Glucose. *J. Chromatogr., A* **2000**, *868*, 169.

(5) Ma, Z.; Wang, N.-H. L. Standing Wave Analysis of SMB Chromatography: Linear Systems. *AIChE J.* **1997**, *40* (10), 2488.

(6) Xie, Y.; Wu, D.; Ma, Z.; Wang, N.-H. L. Extended Standing Wave Design Method for Simulated Moving Bed Chromatography: Linear Systems. *Ind. Eng. Chem. Res.* **2000**, *39*, 1993.

(7) Ruthven, D. M.; Ching, C. B. Counter-current and Simulated Counter-current Adsorption Separation Processes. *Chem. Eng. Sci.* **1989**, *44* (5), 1011.

(8) Juke, A.; Epping, A.; Schmidt-Traub, H. Optimal Design of Batch and Simulated Moving Bed Chromatographic Separation Processes. *J. Chromatogr., A* **2002**, *944*, 93.

(9) Wooley, R.; Ma, Z.; Wang, N.-H. L. A Nine-Zone Simulated Moving Bed for the Recovery of Glucose and Xlyose from Biomass Hydrolyzate. *Ind. Eng. Chem. Res.* **1998**, *37*, 3699.

(10) Petzold, L. R. *DASSL: A Software Package for the Solution of Differential/Algebraic Systems of Equations*; Sandia National Laboratories, Livermore, CA, 1991.

(11) Melis, S.; Markos, J.; Cao, G.; Morbidelli, M. Separation between Amino Acids and Inorganic Ions through Ion Exchange: Development of a Lumped Model. *Ind. Eng. Chem. Res.* **1996**, *35*, 3629.

(12) Dunnebier, G.; Weirich, I.; Klatt, K.-U. Computationally Efficient Dynamic Modeling and Simulation of Simulated Moving Bed Chromatographic Processes with Linear Isotherms. *Chem. Eng. Sci.* **1998**, *53* (14), 2537.

(13) Lim, Y. I.; Le Lann, J. M.; Joulia, X. Accuracy Temporal Performance and Stability Comparisons of Discretization Methods for the Solution of Partial Differential Equations (PDEs) in the Presence of Steep Moving Fronts. *Comput. Chem. Eng.* **2001**, *25*, 1483.

(14) Lim, Y. I.; Jørgensen, S. B. A Fast and Accurate Numerical Method for Solving Simulated Moving Bed (SMB) Chromatographic Separation Problems. *Chem. Eng. Sci.* **2004**, *59* (10), 1931.

(15) Chang, S. C. The Method of Space−Time Conservation Element and Solution Element-A New Approach for Solving the Navier−Stokes and Euler Equations. *J. Comput. Phys.* **1995**, *119*, 295.

(16) Chang, S. C. Courant Number Insensitive CE/SE Schemes. Presented at the 38th AIAA Joint Propulsion Conference, Indianapolis, IN, 2002, Paper No. AIAA-2002-3890.

(17) Lim, Y. I.; Chang, C. S.; Jørgensen, S. B. A Novel Partial Differential Algebraic Equation (PDAE) Solver: Iterative Conservation Element/Solution Element (CE/SE) Method. *Comput. Chem. Eng.* **2004**, *28* (8), 1309.

(18) Knudsen, K. C. The Production of NPK Fertilizers by Ion-Exchange. *J. Appl. Chem. Biotechnol.* **1974**, *24*, 701.

(19) Lim, Y.-I.; Lee, A. L. Simulation of a Six-Zone Simulated Moving Bed Chromatographic Process for NPK Fertilizer Production, *Kor. Chem. Eng. Res.* **2007**, *45* (1), 1.

(20) Migliorini, C.; Mazzotti, M.; Morbidelli, M. Simulated Moving Bed Units with Extra-Column Dead Volume. *AIChE J.* **1999**, *45* (7), 1411.

(21) Mackenzie, J. A.; Robertson, M. L. The Numerical Solution of One-Dimensional Phase Change Problems Using an Adaptive Moving Mesh Method. *J. Comput. Phys.* **2000**, *161* (2), 537.

(22) Lim, Y. I.; Christensen, S.; Jørgensen, S. B. A Generalized Adsorption Rate Model Based on the Limiting-Component Constraint in SMB Chromatographic Separation. In *European Symposium on Computer-Aided Chemical Engineering 13*; Kraslawski, A., Turunen, I., Eds.; Elsevier Science B.V.: Amsterdam, 2003; p 767.

(23) Marcussen, L. Multicomponent Adsorption of Ions from Concentrated Solutions, Superfos-DTU internal report, Department of Chemical Engineering, DTU, Lyngby, Denmark, 1985.

(24) Smith, R. P.; Woodburn, E. T. Prediction of Multicomponent Ion Exchange Equilibria for the Ternary System $SO_4^{2-}-NO_3^{-}-Cl^{-}$ from Data of Binary Systems. *AIChE J.* **1978**, *24* (4), 577.

(25) Molls, T.; Molls, F. Space−Time Conservation Method Applied to Saint Venant Equations. *J. Hydraulic Eng.* **1998**, *124* (5), 501.

(26) Mazzotti, M.; Storti, G.; Morbidelli, M. Optimal Operation of Simulated Moving Bed Units for Nonlinear Chromatographic Separations. *J. Chromatogr., A* **1997**, *769*, 3.

(27) Strube, J.; Altenhoner, U.; Meurer, M.; Schmidt-Traub, H.; Schulte, M. Dynamic Simulation of Simulated Moving-Bed Chromatographic Processes for the Optimization of Chiral Separations. *J. Chromatogr., A* **1997**, *769*, 81.

(28) Mao, G.; Petzold, L. R. Efficient Integration over Discontinuities for Differential−Algebraic Systems. *Comput. Math. Appl.* **2002**, *43*, 65.

(29) Storti, G.; Masi, M.; Paludetto, R.; Morbidelli, M.; Carra, S. Adsorption Separation Processes: Countercurrent and Simulated Countercurrent Operations. *Comput. Chem. Eng.* **1998**, *12* (5), 475.

(30) Lim, Y. I. An Optimization Strategy for Nonlinear Simulated Moving Bed Chromatography: Multi-Level Optimization Procedure (MLOP). *Kor. J. Chem. Eng.* **2004**, *21* (4), 836.

Received for review October 26, 2006
Revised manuscript received February 10, 2007
Accepted February 19, 2007

IE0613772